https://doi.org/10.31436/iiumej.v27i1.3898

Performance Investigation and Efficiency Enhancement of Eco-Friendly Tin-Based CH3NH3SnI3 Perovskite Solar Cell via SCAPS-1D

MD. MORSALIN[1*], RAGAB A. SAYED[2*], MD. SAZEDUR RAHMAN[1], MD. FERDOUS WAHID[1], MOHAMMAD SALAH[3]

[1]Department of Electrical and Electronic Engineering, Hajee Mohammad Danesh Science and Technology University, Dinajpur 5200, Bangladesh.
[2]Automotive and Tractors Technology Department, Faculty of Technology and Education, Capital University – Helwan Branch, Cairo, Egypt.
[3]College of Engineering and Technology, American University of the Middle East, Kuwait.

**Corresponding author: mdmorsalin.hstu@gmail.com, ragab.mahmoud@techedu.helwan.edu.eg*

(Received: 12 August 2025; Accepted: 17 November 2025; Published online: 12 January 2026)

ABSTRACT: Halide perovskite materials, particularly lead-based $CH_3NH_3PbI_3$, have garnered significant attention in the PV industry for their exceptional efficiency in solar cell applications. However, due to the toxicity of lead, research interest has shifted toward Sn-based alternatives. This study explores a lead-free Sn-based perovskite solar cell (PSC) with the structure ITO/TiO_2/$CH_3NH_3SnI_3$/CBTS/Ni, where $CH_3NH_3SnI_3$ ($MASnI_3$) serves as the absorber material, TiO_2 as the electron transport layer (ETL), Cu_2BaSnS_4 (CBTS) as the hole transporting layer (HTL). Device performance is analyzed using the SCAPS-1D simulation software. The impact of key performance-determining parameters, including the thickness, doping density, and defect density of the absorber, ETL, and HTL, has been accounted for. The proposed PSC architecture, optimized for key performance-determining parameters, achieves a power conversion efficiency PCE (η) of 27.28%, an open-circuit voltage (V_{OC}) of 1.0283 V, a fill factor (FF) of 83.62%, and a short-circuit current density (J_{SC}) of 31.72 mA/cm^2. This study examines the influence of interface defect density, shunt and series resistances, back-contact metal work function, and operating temperature on the performance of PSCs. Furthermore, the analysis includes current density-voltage (J-V) and quantum efficiency (QE) characteristics to provide a comprehensive evaluation of the effectiveness of the proposed PSC.

ABSTRAK*:* Bahan perovskit halida, khususnya $CH_3NH_3PbI_3$ berasaskan plumbum, telah menarik perhatian besar dalam industri fotovolta (PV) berikutan kecekapan tinggi dalam aplikasi sel suria; namun, isu ketoksikan plumbum telah mengalih tumpuan penyelidikan kepada alternatif berasaskan timah (Sn). Kajian ini meneroka sel suria perovskit (PSC) bebas plumbum berasaskan Sn dengan seni bina ITO/TiO_2/$CH_3NH_3SnI_3$/CBTS/Ni, di mana $CH_3NH_3SnI_3$ ($MASnI_3$) bertindak sebagai bahan penyerap, TiO_2 sebagai lapisan pengangkut elektron (ETL), dan Cu_2BaSnS_4 (CBTS) sebagai lapisan pengangkut lubang (HTL). Prestasi peranti dianalisa menggunakan perisian simulasi SCAPS-1D dengan mengambil kira parameter penentu prestasi utama, termasuk ketebalan, ketumpatan pendopan, dan ketumpatan kecacatan bagi lapisan penyerap, ETL dan HTL. Seni bina PSC yang dicadangkan, selepas pengoptimuman parameter, mencapai kecekapan penukaran kuasa (PCE) sebanyak 27.28%, voltan litar terbuka (V_OC) 1.0283 V, faktor pengisian (FF) 83.62%, dan ketumpatan arus litar pintas (J_SC) 31.72 mA/cm². Kajian ini turut menilai pengaruh ketumpatan kecacatan antara muka, rintangan siri dan pirau, fungsi kerja logam sentuhan belakang, serta suhu operasi terhadap prestasi PSC. Di samping itu, analisis ciri

ketumpatan arus–voltan (J–V) dan kecekapan kuantum (QE) disertakan bagi memberikan penilaian menyeluruh terhadap keberkesanan sel suria perovskit yang dicadangkan.

KEYWORDS: *Perovskite Solar Cell, CBTS, $MASnI_3$, SCAPS-1D, Solar power.*

1. INTRODUCTION

In the current global energy landscape, fossil fuels remain the dominant source of electricity generation, accounting for a substantial share of worldwide energy demand [1]. Despite their widespread use, the continued reliance on fossil fuels poses several problems, including resource depletion, greenhouse gas emissions, and environmental degradation [2]. These issues have intensified the need for a transition to cleaner, more sustainable energy alternatives. Among the various renewable energy sources, such as wind energy, hydro energy, and ocean energy, solar energy has emerged as a highly promising and scalable solution [3]. Its vast availability, minimal environmental impact, and potential to significantly reduce carbon emissions make it an attractive option for meeting the growing global energy demand [4]. Solar energy, harnessed from the sun's radiation, presents several distinct advantages over other renewable sources. Its abundant availability, geographical accessibility, and potential for decentralized power generation make it a highly attractive option for sustainable energy development [5-7]. With continuous advancements in photovoltaic (PV) technologies, the efficiency and cost-effectiveness of solar energy systems have improved substantially [8,9].

Among the emerging PV technologies, perovskite solar cells (PSCs) have attracted considerable attention in photovoltaic (PV) research owing to their exceptional efficiency in converting photon energy into electricity, as well as their beneficial electrical properties [10]. Perovskite materials are distinguished by their excellent properties, including longer diffusion lengths, high absorption coefficients, superior charge carrier mobility, and relatively low exciton binding energy, making them highly suitable for solar energy applications [11-13]. In the middle of the 1990s, Mitzi et al. first discovered the ability of electricity to convert light in halide perovskites, applied to LEDs [14].

In 2009, Kojima et al. first illustrated the dye-sensitized solar cell [15] structures with $CH_3NH_3PbI_3$ and achieved an efficiency of 3.8% [16]. Halide perovskites are materials characterized by the formula "ABX_3" [17], where "A" represents monovalent cations (Cs^+, $CH_3NH_3^+$, $CH(NH_2)_3^+$), "B" denotes cationic metals like Sn^{2+} or Pb^{2+}, and "X" corresponds to halogen ions (Cl^-, I^-, Br^-). $MAPbI_3$ (methylammonium lead triiodide) is the predominant perovskite material used in solar cells (SCs). However, the presence of lead raises significant concerns regarding its toxicity [18]. In contrast, tin-based perovskites, such as methylammonium tin iodide (MASnI3), offer a more environmentally friendly and safer alternative for commercialization due to tin's non-toxicity. Furthermore, tin-based perovskites also exhibit properties comparable to those of lead-based counterparts while reducing expenses, facilitating a seamless adaptation of existing manufacturing processes [19, 20]. Replacing lead with tin creates a material with a specific light absorption property (bandgap) very close to the actual value for SCs, as claimed by the Shockley-Queisser limit [20]. This characteristic makes tin-based perovskites promising for making high-efficiency SCs, especially when combined with other perovskite materials [19].

In this investigation, a tin-based and lead-free PSC device structure of $ITO/TiO_2/CH_3NH_3SnI_3/CBTS/Ni$ is proposed and simulated using SCAPS-1D software. It shows the short-circuit current density (J_{SC}) 31.7233 mA/cm^2, efficiency (η) 27.28%, fill factor (FF) 83.62%, and open-circuit voltage (V_{OC}) 1.0283 V. These findings demonstrate superior

performance compared to previously reported studies [21-24]. Here, a transparent conducting oxide, indium-doped tin oxide (ITO), [25], is considered as a transparent glass in front contact, while Nickel (Ni) is considered as a back metal contact in the PSC device. Additionally, TiO2 is used as an electron transport layer (ETL) because its conduction band (CB) [26] is similar to that of perovskites, and it has good optical and chemical stability, non-toxicity, and an easy manufacturing process [21,22].

A lead-free tin-based perovskite ($CH_3NH_3SnI_3$) is used as an absorber material because of its appropriate bandgap, non-toxicity, and inexpensive, earth-abundant, high absorption coefficient [21]. Copper barium tin sulfide (CBTS) is taken as a hole transport layer (HTL) because of its hole mobility, high stability, and excellent bandgap alignment with the $CH_3NH_3SnI_3$ absorber. Its high hole mobility efficiently transports positive charges (holes) from the light-absorbing layer (perovskite) toward the electrode [27]. This improves overall device efficiency by minimizing charge recombination within the cell. The proper selection of ETLs and HTLs enhances the performance and efficiency of the SC device. In this study, we examined the effects of varying the thickness, donor and doping densities, and trap densities (Nt) of the HTL, ETL, and absorber layers, as well as interface defect densities, on the quantum efficiency (QE) and current-voltage (J-V) characteristics. Additionally, we analyzed the effects of operating temperature, shunt and series resistances, and the work function (WF) of the back contact metal. Furthermore, we investigated how variations in these parameters affect the performance of the PSC device without an HTL.

2. METHODOLOGY

2.1. SCAPS-1D numerical simulation

The SCAPS-1D (version 3.3.10) software is used in this study to investigate the photovoltaic (PV) parameters. The software is provided by Prof. Marc Burgelman et al. at the ELIS department [25], Ghent University, Belgium [25,26]. SCAPS-1D software operates based on solving numerical equations, such as the continuity equation for holes and electrons [30] in the CB and VB [21] and the Poisson's equation. The Poisson's (Eq. (1)) [31] and continuity equations [32] (Eq. (2) for electrons and Eq. (3) for holes) are depicted below:

$$\frac{d^2}{dx^2}\psi(x) = \frac{q}{\varepsilon_0 \varepsilon_r}\left[p(x) - n(x) + N_D - N_A + \rho_p + \rho_n\right] \quad (1)$$

$$\frac{\partial n}{\partial t} = \frac{1}{q}\frac{\partial J_n}{\partial x} + (G_n - R_n) \quad (2)$$

$$\frac{\partial p}{\partial t} = \frac{1}{q}\frac{\partial J_p}{\partial x} + \left(G_p - R_p\right) \quad (3)$$

where, ε_0 stands for the permittivity of free space, ψ represents the electric potential, ε_r stands for the relative permittivity, p(x) and n(x) represent the hole and electron densities respectively, ρ_n represents electron distribution and ρ_p represents the hole distribution, N_D and N_A represent the donor and acceptor densities, respectively, J_p and J_n stand for the current densities [33] for electrons and holes, respectively, G_p and G_n stand for the holes and electrons generation, respectively, R_p and R_n represent the holes and electrons recombination, respectively, and q represents the electric charge. The simulation is conducted under illumination using an AM 1.5G solar spectrum at a power density of 1000W/m^2.

Table 1. Input parameters of the ITO, Absorber, HTL, and ETL layers.

Parameters	ITO [26]	TiO_2 [26]	$CH_3NH_3SnI_3$[21]	CBTS [26]
Thickness (μm)	0.5	0.03	0.7	0.1
E_g (eV)	3.5	3.2	1.3	1.9
χ (eV)	4	4	4.2	3.6
ε_r (relative)	9	9	8.2[24]	5.4
N_c (cm^{-3})	2.2×10^{18}	2×10^{18}	1×10^{18}	2.2×10^{18}
N_v (cm^{-3})	1.8×10^{19}	1.8×10^{19}	1×10^{18}	1.8×10^{19}
μ_n ($cm^2V^{-1}s^{-1}$)	20	30	1.6	30
μ_p ($cm^2V^{-1}s^{-1}$)	10	10	1.6	10
N_A (cm^{-3})	0	0	1×10^{17}	1×10^{19}
N_D (cm^{-3})	1×10^{21}	6×10^{19}	0	0
N_t (cm^{-3})	1×10^{15}	1×10^{15}	1×10^{15}	1×10^{15}

Here, **E_g:** Bandgap, **χ:** Electron Affinity, **ε_r:** Dielectric permittivity, **N_c:** CB effective DOS, **N_v:** VB effective DOS, **μ_n:** Electron mobility, **μ_p:** Hole mobility, **N_A:** Shallow uniform acceptor density, **N_D:** Shallow uniform donor density, and **N_t:** Defect density.

2.2. Device structure and simulation parameters

The proposed PSC device structure is depicted in Figure 1. The PSC structure consists of ITO/TiO_2/$CH_3NH_3SnI_3$/CBTS/Ni, where $CH_3NH_3SnI_3$ is used as an absorber, p-type CBTS is used as an HTM, and n-type TiO_2 is used as an ETM. The energy band diagram (EBD) of the proposed PSC device is shown in Figure 2.

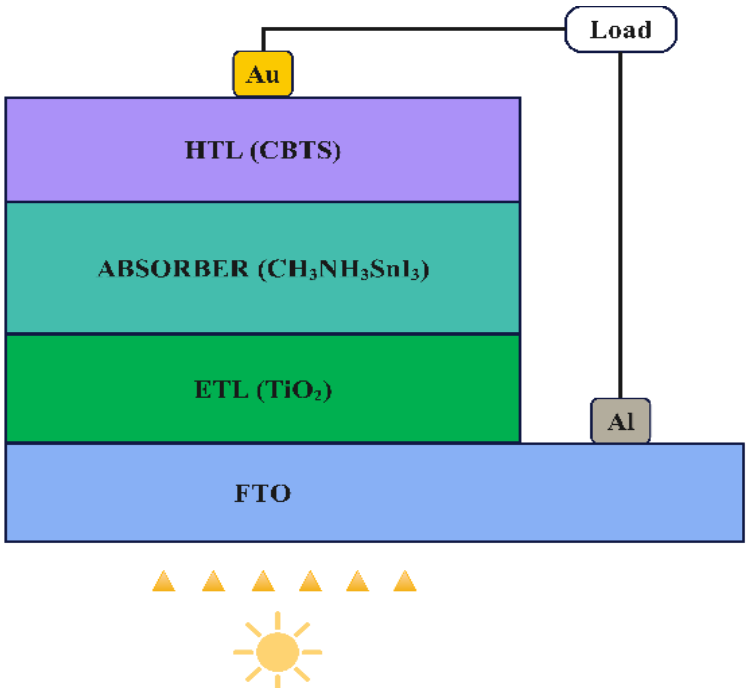

Figure 1. The device structure of the proposed PSC.

When light shines on the SC [34], it creates energy levels called quasi-Fermi levels [26] (F_p and F_n). This confirms that the light successfully generates electron-hole pairs in the PSC. There is a slight offset in the CB/VB of the absorber layer observed from the energy band diagram in Figure 2, which facilitates the generation of electron-hole pairs [35] in the SC. There is also a slight offset in the CB/VB between the absorber layer, the HTL, and the ETL. However, an excessively large offset can introduce resistance that reduces the cell's FF. A mismatch between the materials' energy levels likely accounts for the larger difference.

https://doi.org/10.31436/iiumej.v27i1.3898

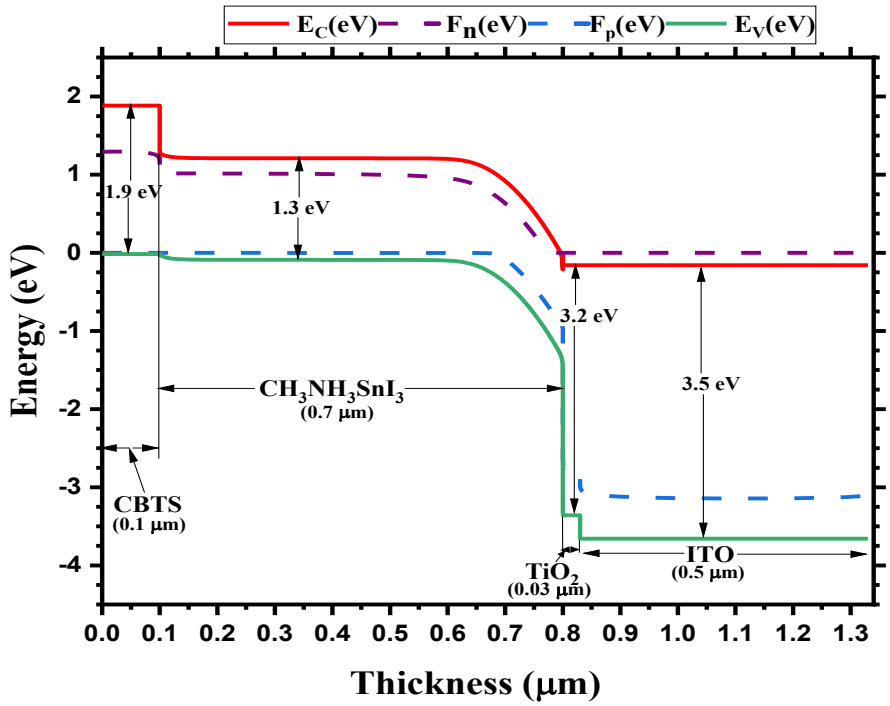

Figure 2. The energy band diagram (EBD) of the proposed PSC.

Table 2. Parameters for interface defects [36].

Parameters	CBTS/CH3NH3SnI3 interface	CH3NH3SnI3/TiO2 interface
Defect type	Neutral	Neutral
Capture cross-sector: electron	1×10-15	1×10-15
Capture cross-sector: hole	1×10-15	1×10-15
Energetic distribution	Single	Single
Reference for defect energy level	Above the highest EV	Above the highest EV
Total density (cm-2)	1×10-11	1×10-11

The input parameters that are used in this simulation, such as thickness, bandgap, electron affinity, mobility for electrons and holes, relative permittivity, acceptor and donor densities, the effective density of states (DOS) in the valence bands (VB), and conduction bands (CB), total defect densities of HTL, absorber, and ETL are given in Table 1. The interfacial defects between absorber/HTL and ETL/absorber are also presented in Table 2. The performance of the designed SC is evaluated across different temperatures to investigate how the device's efficiency varies with temperature. However, a temperature of 300 K (room temperature) is considered throughout the study as the standard reference, since it represents the typical operating environment of PSCs under normal laboratory and ambient conditions, ensuring consistency and comparability of performance parameters [37].

3. RESULTS AND DISCUSSIONS

3.1. Absorber layer thickness variation effect on PV performance

The absorber-layer thickness in perovskite solar cells governs light absorption and recombination dynamics, thereby indirectly influencing the diffusion length and lifetime of charge carriers and ultimately determining device performance [38,39]. An overly thick absorber layer leads to increased recombination and series resistance, whereas an insufficiently thick layer compromises photon absorption and photocurrent [40-43]. Therefore, optimizing

the absorber layer thickness is essential for maximizing SC efficiency. This study investigates the effects of varying absorber layer thickness from 0.1µm to 1.8µm, with Nt = 1015 cm-3, on the performance of the proposed solar cell device for configurations with and without an HTL, as illustrated in Figure 3(a). The η and Jsc increased with thickness up to 0.7 µm. At this thickness, the η and Jsc were 27.28% and 31.72 mA/cm² with HTL, and 24.63% and 29.44 mA/cm² without HTL. This increase is attributed to enhanced light absorption, resulting in the generation of electron-hole pairs within the absorber layer [44]. Increasing the absorber thickness above 0.7 µm leads to recombination and series resistance that limit further improvements in η and Jsc. Figure 3(a) indicates that the FF initially increases with small thickness increments but decreases with further increases in thickness for both configurations, due to increased series resistance. Moreover, the open-circuit voltage of the device with HTL decreases with increasing thickness, attributed to increased recombination of free charge carriers [45]. In the absence of an HTL, Voc increases. This is attributed to the fact that as the absorber thickness increases, both the photon absorption capacity and the rate of charge-carrier generation rise, facilitating their transport to the electrode with reduced resistance [46]. Consequently, the findings establish 0.7 µm as the optimal absorber thickness for further investigation.

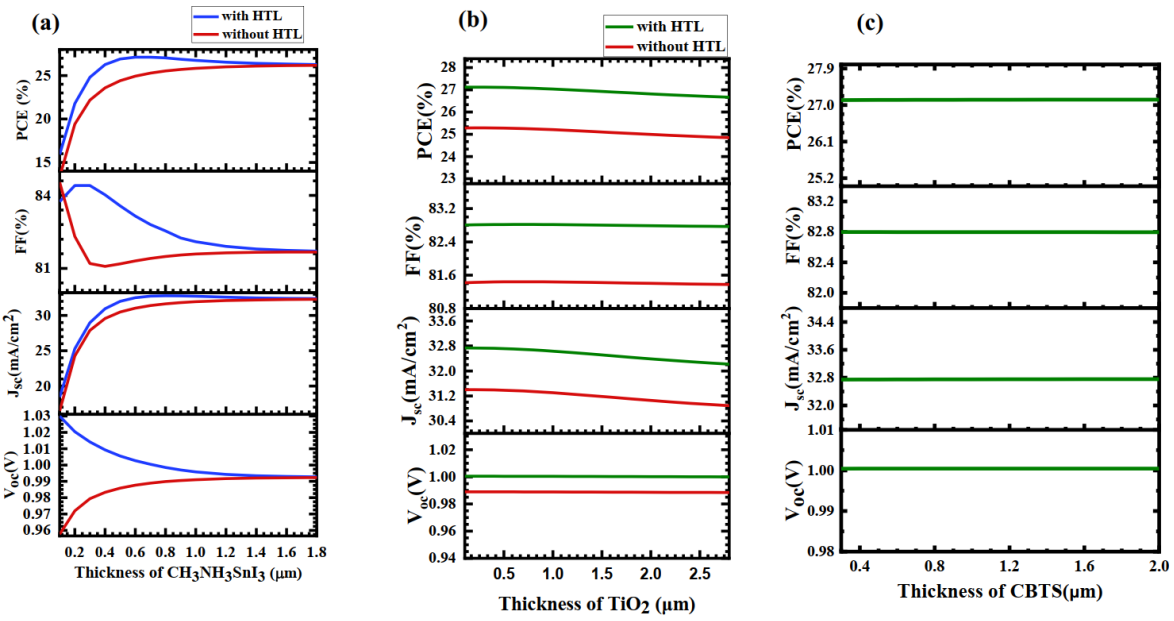

Figure 3. (a) the absorber layer thickness change, (b) the TiO_2 (ETL) layer thickness change, and (c) the HTL layer thickness change on PV performance for both devices with and without HTL.

3.2. ETL thickness variation effect on PV performance

ETL plays a crucial role in facilitating electron transfer from the absorber layer to the electrode. Figure 3(b) illustrates the influence of ETL thickness on the performance of devices with and without HTL. ETL thickness was systematically varied from 0.1 µm to 3 µm, with all other device parameters held constant. The analysis revealed insignificant variation in PV output parameters across the examined range of ETL thicknesses. However, a slight reduction in both Jsc and η is observed as the ETL thickness increases, regardless of HTL presence. This behavior is primarily due to the lower absorption coefficient and decreased light transmittance through the device as the ETL layer increases in thickness [26,47]. Therefore, based on the observed results, a thickness of 0.03 µm is selected as the optimal ETL thickness.

https://doi.org/10.31436/iiumej.v27i1.3898

3.3. HTL thickness variation effect on PV performance

This study evaluates the performance of the proposed PSC by analyzing the impact of HTL thickness variation on output parameters, emphasizing its role in facilitating efficient hole collection from the absorber layer, as depicted in Figure 3(c). Variations in HTL thickness from 0.3 µm to 2 µm produced negligible changes in PV output parameters. This is attributed to the high absorption coefficient of CH3NH3SnI3 and its reduced sensitivity to variations in HTL thickness [48,49]. However, a thicker HTL enhances photon collection in the perovskite layer; therefore, an optimized HTL thickness of 0.1 µm was chosen for subsequent optimization, consistent with the initial study parameters.

3.4. Absorber acceptor and defect density variation effect on PV performance

To determine the effect of absorber acceptor density (N_A) on the PV performance, the N_A of the $CH_3NH_3SnI_3$ layer was changed between 10^{14} cm^{-3} and 10^{18} cm^{-3}. Figure 4(a) shows the changes in J_{SC}, η, V_{OC}, and FF of devices with and without an HTL absorber as the absorber NA varies. As delineated in Figure 4(a), V_{OC} increases with the increase in N_A and is obtained at 1.085V with the HTL and 1.073V without the HTL device at the N_A of 10^{18} cm^{-3}. Conversely, η and FF increase notably with NA in both configurations, with and without HTL. For the HTL-equipped device, FF increased from 79.65% to 85.730% and η from 25.08% to 27.65%, and for the configuration without HTL, FF increased from 80.00% to 85.18% and η from 25.04% to 24.54%.

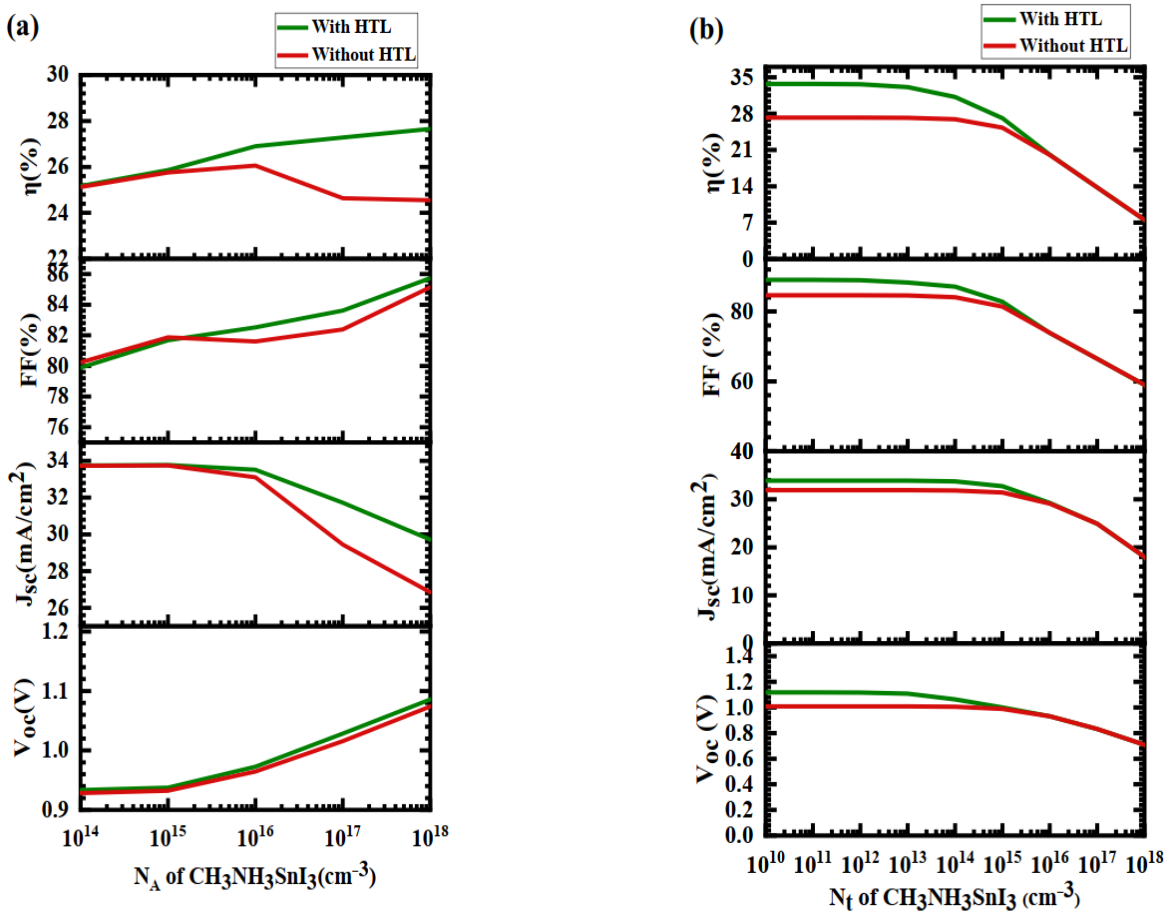

Figure 4. The effect of (a) acceptor density (N_A) and (b) defect density (Nt) of the absorber layer on PV performance for both devices with and without HTL

With the increase in N_A, the reverse saturation current decreases, which increases V_{OC} [21] and hence contributes to FF and η enhancement [36]. The J_{SC} decreases with increasing absorber-layer NA, decreasing from 33.747 mA/cm2 to 29.712 mA/cm2 for the HTL device and from 33.72 mA/cm2 to 26.849 mA/cm^2 for the device without HTL. This decrease in J_{SC} is because the higher carrier density will increase the recombination process and reduce the probability of collecting electrons generated from photons [50]. So, to get the best performance of η= 27.28%, J_{SC}= 31.7233 mA/cm^2, FF= 83.62%, and V_{OC}= 1.0283 V, the optimum value of N_A is taken as 1×10^{17} cm^{-3}. Similarly, the influence of absorber defect density (N_t) has been investigated in this study, as shown in Figure 4(b). The N_t in the absorber layer of an SC significantly affects its performance. Defects in this layer can trap charge carriers, leading to recombination and reduced efficiency [51]. The η, J_{SC}, FF, and V_{OC} decreased considerably with increasing Nt in the absorber for both configurations with and without HTL, as shown in Figure 4(b). At defect densities ranging from 1010 cm-3 to 1013 cm-3, device performance remained relatively unchanged. This suggests that a certain level of defects can be tolerated within the absorber layer without significantly impacting device functionality. However, when N_t exceeds 10^14 cm-3, the devices' output performance begins to decline gradually. This decline is primarily attributed to the Shockley-Read-Hall (SRH) non-radiative recombination process [26,52]. The equations define it.

$$R_{SRH} = \frac{[n_p - n_i]}{[\tau\left(\mathrm{p+n+}\frac{2n_i(E_i-E_t)}{kT}\right)]} \tag{4}$$

$$\tau = \frac{1}{[\sigma\times \mathrm{Nt}\times V_{th}]} \tag{5}$$

Here, σ stands for the charge carriers' capture cross-section, τ for their lifetime, and Vth for their normal velocity. By increasing the crystallinity of the crystalline perovskite and utilizing suitable processing settings that can lower SRH recombination [26,53], it is possible to decrease the number of defects in the material. In this analysis, the optimized N_t is set to 1015 cm-3 for subsequent analysis.

3.5. ETL Donor and defect density variation effect on PV performance

To observe the impact of donor concentration (N_D) variation of ETL on the output performance of the PSC device, N_D of ETL varied from 10^{14} cm^{-3} to 10^{20} cm^{-3}. Figure 5(a) represents the parameters, including η, J_{SC}, FF, and V_{OC}, as a function of the donor density (N_D) of the ETL layer. No significant change in the output parameters was observed with variations in the ETL ND; however, all parameters increased slightly for both configurations with and without an HTL. Because a larger value of N_D of ETL makes the charge carrier extraction and transmission easier in the absorber/ETL interface [54]. The V_{OC} is constant and independent of N_D because the recombination rate is unaffected [54]. In these scenarios, we considered the optimized N_D of ETL to be 6×10^{19} cm^{-3} with the consideration of CB density of states as Table I and shows the output parameters η= 27.28%, J_{SC}= 31.7233 mA/cm^2, FF= 83.62%, and V_{OC}= 1.0283 V. Figure 5(b) showcases the influence of defect density (N_t) of the TiO_2 (ETL) on the output parameters of devices with and without HTL. Interestingly, as N_t of ETL increased across a range of 10^{10} cm^{-3} to 10^{18} cm^{-3}, all the performance parameters remained relatively unchanged for both configurations, as shown in previous works [26,55]. Consequently, we selected 10^{15} cm^{-3} as the optimal N_t for the ETL in this study.

https://doi.org/10.31436/iiumej.v27i1.3898

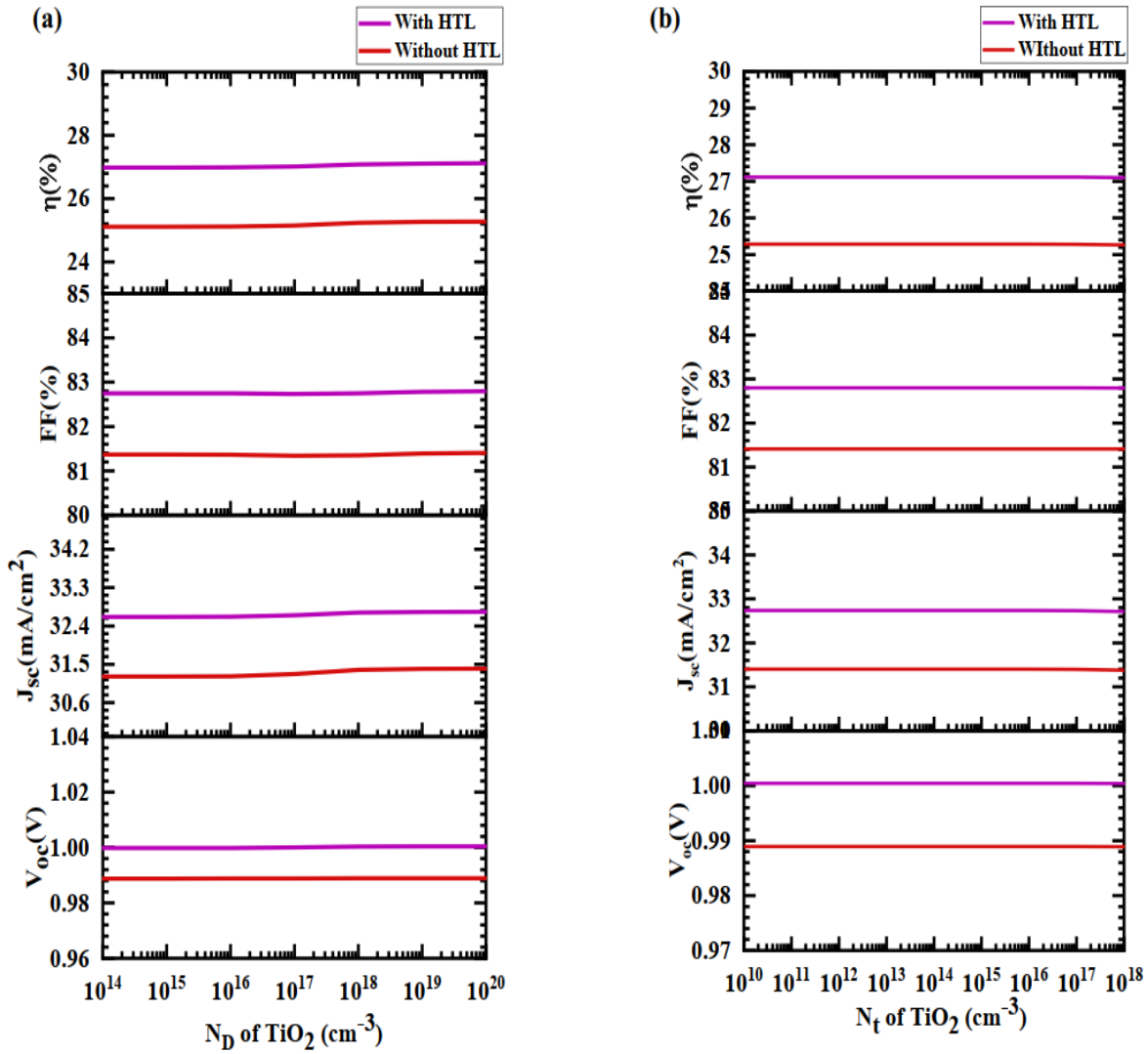

Figure 5. (a) Donor concentration (N_D) and (b) defect density (N_t) of the ETL on PV performance for the devices with and without HTL.

3.6. HTL Acceptor and defect density variation effect on PV Performance

The acceptor density (N_A) in the HTL of SC refers to the concentration of acceptor atoms or molecules within the HTL material. Acceptor dopants introduce additional energy levels near the VB of the semiconductor, providing free positive charge carriers [36]. Figure 6(a) delineates the effect of N_A of the HTL on the PV performance of the PSC as N_A is varied from 10^{10} cm^{-3} to 10^{20} cm^{-3}. In this study, the J_{SC}, FF, V_{OC}, and η remained essentially constant up to 10^{16} cm^{-3} of HTL's N_A. When the value of N_A of HTL exceeds 10^{16} cm^{-3}, all the parameters slightly increase.

https://doi.org/10.31436/iiumej.v27i1.3898

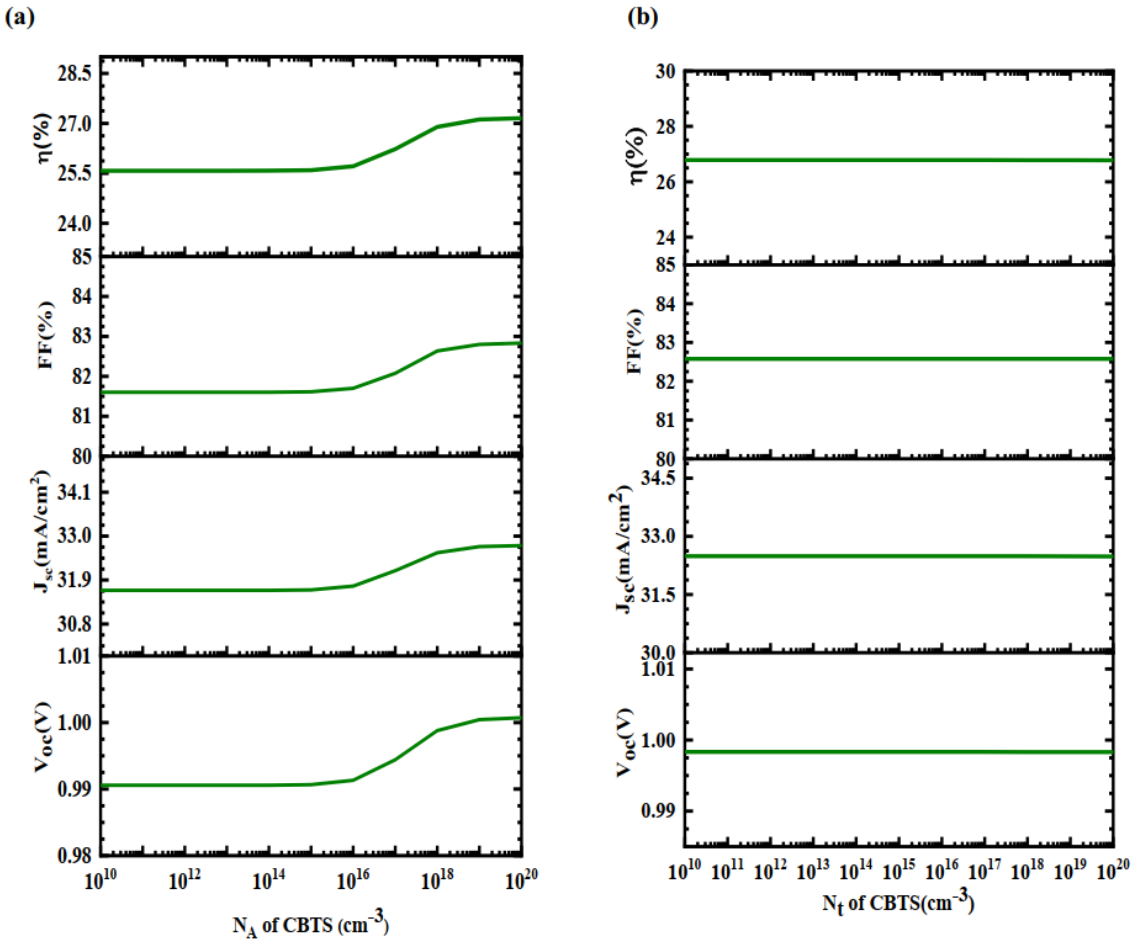

Figure 6. (a) N_A and (b) N_t of HTL on PV performance

Here, the built-in voltage at the absorber/HTL interface increases as the N_A of the HTL increases because the VB of the HTL approaches the quasi-Fermi level [56]. As the N_A of HTL increases, the rate of recombination of electron-hole pairs decreases, which in turn reduces the series resistance and increases the shunt resistance; as a result, FF increases and enhances the overall efficiency [56]. To improve performance, we select the NA of HTL as 1019 cm-3 for subsequent simulations. Similarly, Figure 6(b) illustrates the changes in output parameters as the defect density (N_t) of the CBTS is increased from 10^{10} cm^{-3} to 10^{20} cm^{-3}. Interestingly, η, FF, V_{OC}, and J_{SC} exhibit minimal variation across the entire range of N_t variation. This finding aligns with prior research on CBTS HTL, reinforcing the stability of PV parameters irrespective of N_t fluctuations [26,57-59]. Thus, we determine the primary value of 1015 cm-3 as the optimal Nt for the HTL layer in this study.

3.7. Interface defect density variation effect on PV parameters

This simulation investigated how the PV performance of the proposed SC is affected by defect density (Nt) at the critical TiO2/CH3NH3SnI3 and CH3NH3SnI3/CBTS interfaces, as shown in Figs. 7(a) and 8(b). The interface defect densities were varied across a wide range, from 10^{10} cm^{-2} to 10^{16} cm^{-2} for $TiO_2/CH_3NH_3SnI_3$ interface and from 10^{7} cm^{-2} to 10^{16} cm^{-2} for $CH_3NH_3SnI_3$/CBTS interface. A consistent pattern emerged from the data analysis: FF, η, VOC, and JSC decreased in parallel with increasing N_t at both interfaces. Higher concentrations of interfacial defects are associated with increased recombination rates, which may be the cause of the reduction in PV performance [60]. Interestingly, our findings indicate that the N_t at the

https://doi.org/10.31436/iiumej.v27i1.3898

$CH_3NH_3SnI_3$/CBTS interface exerts a greater influence on device efficiency than at the TiO_2/$CH_3NH_3SnI_3$ interface. Consequently, we maintained a trap density of 10^{10} cm^{-2} at both interfaces, consistent with our initial selection. This choice ensures optimal device performance while mitigating the adverse effects of interfacial defects on recombination and charge transport within the SC.

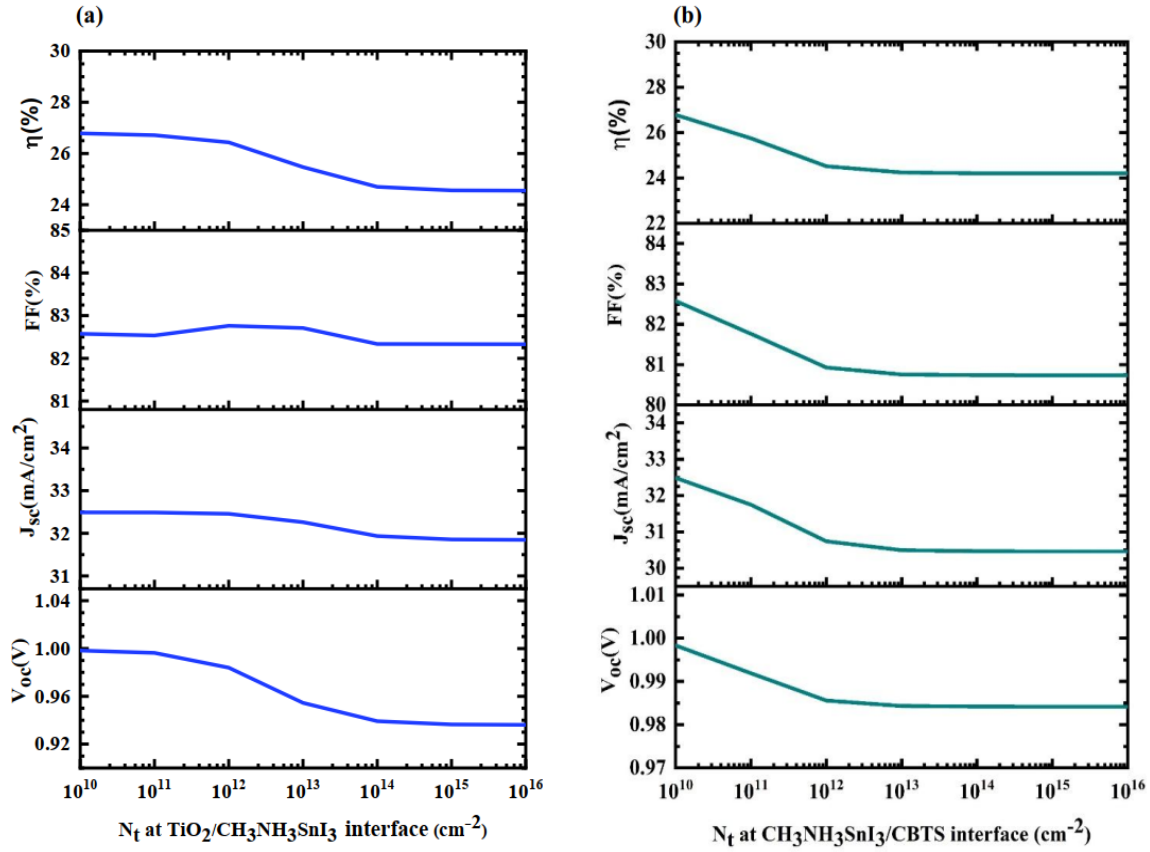

Figure 7. The influence of N_t variation (a) at the TiO_2/$CH_3NH_3SnI_3$ interface and (b) at the $CH_3NH_3SnI_3$/CBTS interface on PV performance

3.8. The J-V and QE features

The J-V (current density-voltage) curve of a solar cell displays distinct characteristics that indicate optimal performance. Figure 8(a) illustrates the anticipated relationship between current density (J) and voltage (V) for both device configurations, with and without HTL. In both devices, the current density decreases with the increase in voltage (V), which shows a similar trend to the previous works [61,62]. Quantum efficiency (QE), also sometimes called the incident photon-to-converted electron (IPCE) ratio, is a measure of how effectively a SC device converts light into usable electrical current [63]. Greater QE of an SC results in more sunlight being converted into electricity. A device might have a high QE for visible light but a lower QE for infrared or ultraviolet light. Figure 8(b) shows the QE features and wavelength (nm) for the device configurations, with and without HTL. Across the wavelength range of 200–1200 nm, the QE curve initially approaches 100% before gradually decreasing to 0% at 960 nm in both device configurations.

https://doi.org/10.31436/iiumej.v27i1.3898

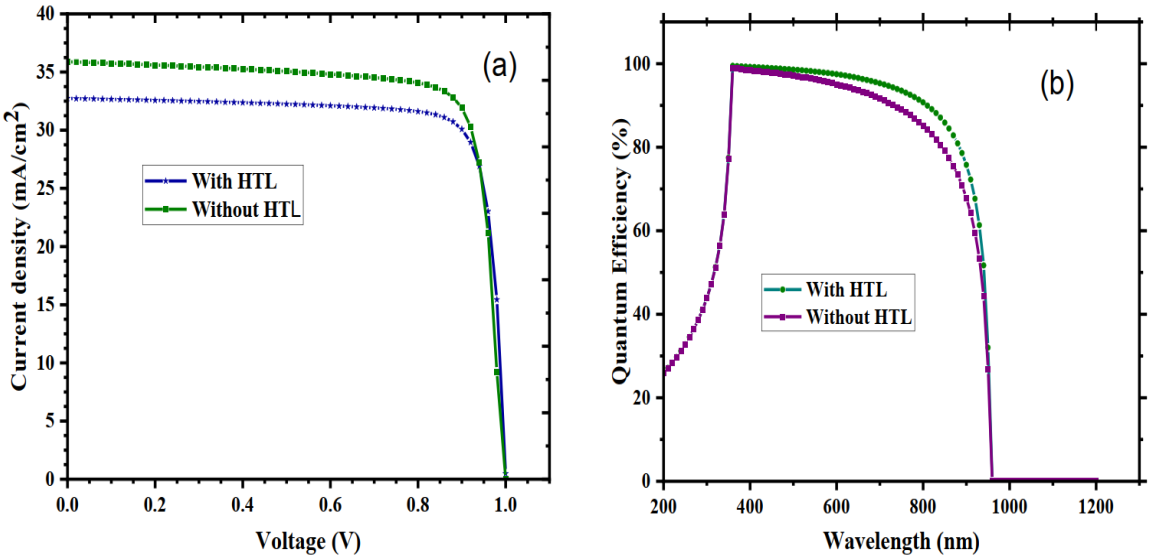

Figure 8. (a) J-V curve and (b) QE curve with and without HTL configurations.

3.9. Series and shunt resistance variation effect on PV performance

Figure 9(a) illustrates the impact of varying series resistance (R_s) on the PV parameters of the devices with and without the HTL.

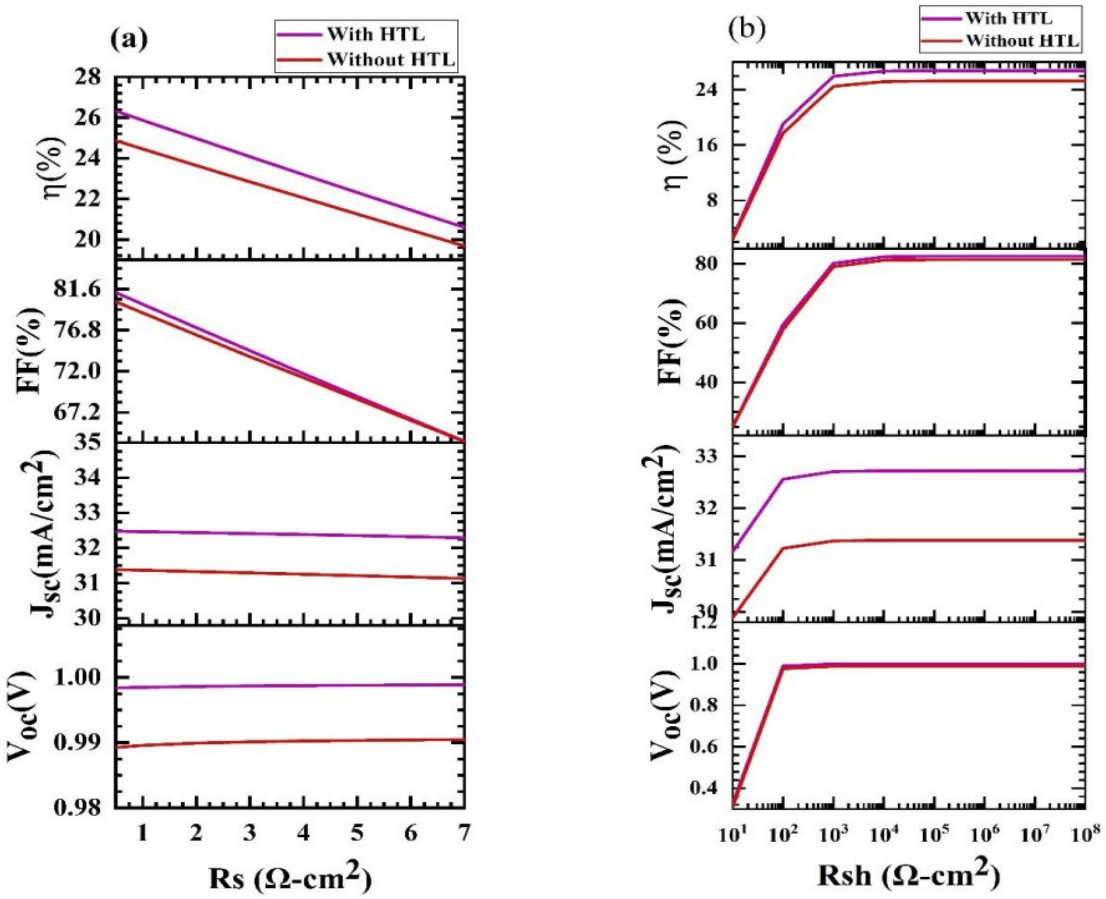

Figure 9. The influence of (a) series resistance and (b) shunt resistance on PV output parameters.

https://doi.org/10.31436/iiumej.v27i1.3898

The R_s values range from 0.5 to 7 Ω-cm², with the shunt resistance (Rsh) of 10^5 Ω-cm². The key observation is that increasing R_s has a minimal effect on VOC and little effect on the JSC of the HTL configuration. However, it negatively affects the other parameters. As Rs increases, FF decreases more markedly, from 82.55% to 63.84%, and η decreases from 26.77% to 20.59% for the device with HTL. For the layout without the HTL configuration, the trends are identical. In essence, higher R_s causes internal power losses within the device, which lowers its overall efficiency. Here, R_s is the total amount of resistance between semiconductor-semiconductor and semiconductor-metal at the rear and front contacts of the SC. Conversely, in the active junction, the reverse saturation current [21], which results from manufacturing defects, generates R_{sh}. Again, Figure 9(b) depicts the influence of R_{sh} on the PV parameters for devices with and without HTL. R_{sh} ranges from 10 to 108 Ω-cm², with a series resistance of 0.5 Ω-cm². The results show that increasing R_{sh} increases JSC, VOC, η, and FF for both devices within a specific Rsh range. When R_{sh} exceeded 10^3 Ω-cm^2, the investigation found a saturation in all output parameters. Higher R_{SH} signifies reduced leakage current within the device [64], leading to improved overall effectiveness of the SC. Thus, our study suggests that both resistances considerably influence the SC's PV performance.

3.10. Temperature and back contact metal variation effect on PV performance

The effect of temperature variation on the photovoltaic performance of the designed PSC is analyzed for both configurations, as shown in Figure 10(a). Except for the J_{SC}, all parameters decreased significantly as the temperature was increased from 275 K to 425 K in both devices with and without an HTL. The steady decline in device performance as temperature rises can be attributed to the concurrent increase in deformation stress and defects, consistent with previous findings [65]. Additionally, high temperatures significantly affect the diffusion length [66] and cause an increase in series resistance (RS), thereby directly affecting the device's η and FF. Again, various metal contacts Gold (Au), Carbon (C), Selenium (Se), Copper (Cu), Nickel (Ni), Palladium (Pd), Iron (Fe), and Platinum (Pt) are used in this simulation to find the effect of back metal variation on PV performance which is shown in Figure 10(b).

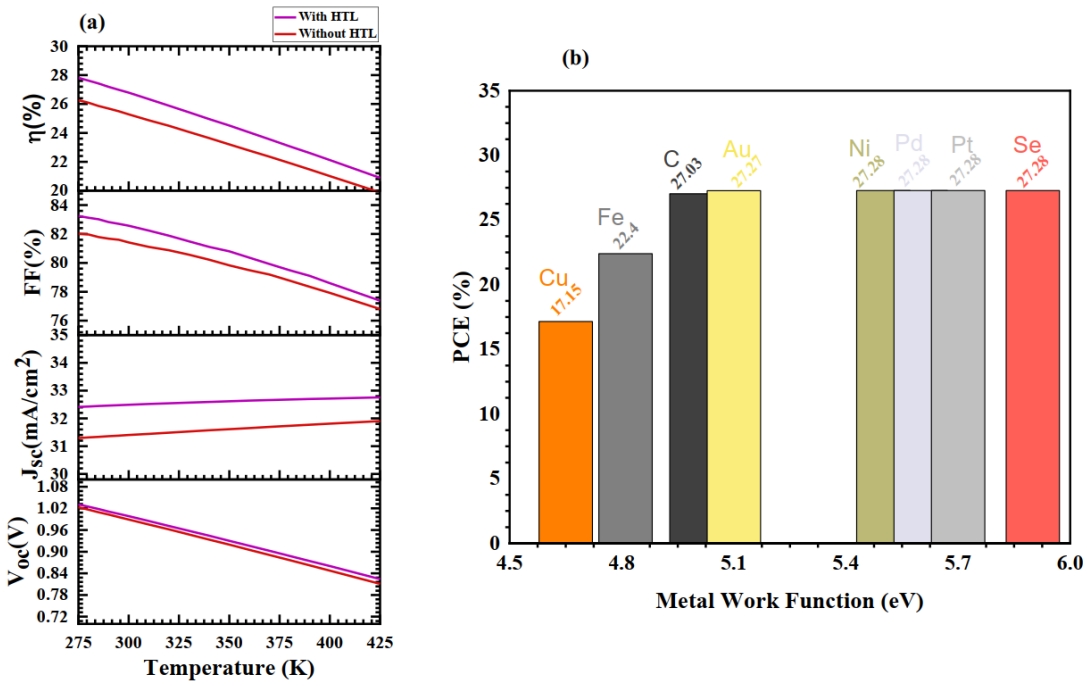

Figure 10. (a) The effect of temperature variation, and (b) Bar diagram for the back metal's WF (eV) variation effect on PV performance.

The bar diagram indicates that the structure's η increases with the metal contact work function (WF) and saturates above 5.1 eV. The enormous barrier formed by the lower WF (eV) materials at the rear side [67] prohibits the entire transit from the absorber to the back metal contact, resulting in low PV output parameters. It becomes apparent that the back contact metal's WF has an essential impact on the performance of SCs. Based on the current investigation outcomes, it is recommended that a back metal with a WF larger than 5.1 eV is necessary to achieve optimal PV performance. Due to its inexpensive cost and suitable WF, nickel (Ni) was chosen as the back metal contact material in this study [68].

3.11. Comparison of the investigated results with previous works

This section compares several optimal solar cell configurations. Table 3 presents a comparative overview of recent theoretical and experimental studies on CH3NH3SnI3-based PSC devices, along with our results.

Table 3. The comparison of $CH_3NH_3SnI_3$-based PSCs

Device structures	Ref.	V_{OC}	J_{SC}	FF	η(%)
(a) FTO/TiO2/CH3NH3SnI3/CZTSe	[69]	0.86	29.45	76.74	19.52
(b) FTO/TiO2/CH3NH3SnI3/CZTSe	[70]	0.96	32.48	76.40	23.86
(c) FTO/Cd0.5Zn0.5S/MASnI3/MASnBr3	[23]	1.055	34.268	69.23	25.05
(d) FTO/ PCBM/MASnI3/CuI	[71]	0.83	29.71	61.23	15.10
(e) FTO/ZnO/CH3NH3SnI3/CuO	[72]	0.989	33.863	66.33	22.21
(f) FTO/TiO2/CH3NH3SnI3/Spiro-OMeTAD,	[25]	0.99	32.95	77.77	25.48
(g) FTO/ C60/MASnI3/CuAlO2	[22]	1.08	25.85	85.84	24.04
(h) ITO/TIO2/CH3NH3SnI3/CBTS	This work	1.028	31.723	83.62	27.28

Compared to others, the investigated device structure ITO/TiO_2/$CH_3NH_3SnI_3$/CBTS/Ni obtained the best performance with η=27.28%, J_{SC}= 31.7233 mA/cm^2, FF=83.62%, and V_{OC}= 1.0283 V. This numerical study identified a combination of materials leading to the best performance: CBTS as the HTM, TiO_2 as the ETM, and $CH_3NH_3SnI_3$ as the light absorber. This configuration outperforms the other investigated structures, underscoring the critical role of the light-absorbing layer in SC performance. $CH_3NH_3SnI_3$ has attracted significant research interest owing to its light-absorption properties. However, this study demonstrates that optimizing and carefully selecting both the ETL and HTL, along with their optoelectronic parameters, are crucial for achieving superior solar cell efficiency.

4. CONCLUSION

This research presents a comprehensive simulation approach to investigate the output performance of $CH_3NH_3SnI_3$ ($MASnI_3$)-based PSC. This investigation shows the proposed SC device with the structure ITO/TiO_2/$CH_3NH_3SnI_3$/CBTS/Ni, simulated using the SCAPS-1D software package. During optimization, the absorber ($CH_3NH_3SnI_3$) layer, ETL, and HTL's thickness, defect and dopant densities, interface defect densities, shunt and series resistances, and temperature effects on PSC's performance were considered. After optimization, the following conclusions are obtained. The final optimized thicknesses of the absorber ($MASnI_3$) layer, CBTS (HTL) layer, and TiO_2 (ETL) layer are 700 nm, 100 nm, and 30 nm, respectively, for both devices with and without HTL. The optimal doping concentrations of the absorber of the PSC devices using and not using HTL are 10^{17} cm^{-3} and 10^{16} cm^{-3}, respectively, while the optimized ETL donor, HTL acceptor, and absorber defect densities are 6×10^{19} cm^{-3}, 10^{19} cm^{-3}, and 1×10^{15} cm^{-3}. The finally optimized ITO/TiO_2/$CH_3NH_3SnI_3$/CBTS/Ni structure achieved a

JSC of 31.7233 mA/cm2, an η of 27.28%, a VOC of 1.0283 V, and an FF of 83.62%. Furthermore, we examined the series and shunt resistances, the QE curve, the operating temperature, and the illuminated J-V curve. The QE of the optimized configuration remained constant up to 700 nm and fell toward zero at 960 nm, indicating that photon-to-electron conversion occurs across the entire visible spectrum. A comparative analysis with prior studies confirms that the proposed device architecture achieves superior efficiency among CH3NH3SnI3-based PSCs, underscoring its potential for future eco-friendly, high-performance SC applications.

ACKNOWLEDGEMENT

The authors extend their appreciation to the American University of the Middle East in Kuwait for funding this work. This contribution has been instrumental in facilitating the dissemination of the study's findings.

REFERENCES

[1] T. Ahmad and D. Zhang, "A critical review of comparative global historical energy consumption and future demand: The story told so far," Energy Reports, vol. 6, pp. 1973–1991, 2020, doi: https://doi.org/10.1016/j.egyr.2020.07.020.

[2] M. Höök and X. Tang, "Depletion of fossil fuels and anthropogenic climate change—A review," Energy Policy, vol. 52, pp. 797–809, 2013, doi: https://doi.org/10.1016/j.enpol.2012.10.046.

[3] F. A. Akash, S. M. Shovon, W. Rahman, M. A. Rahman, P. Chakraborty, and M. U. Monir, "Greening the grid: A comprehensive review of renewable energy in Bangladesh," Heliyon, vol. 10, no. 5, Mar. 2024, doi: 10.1016/j.heliyon.2024.e27477.

[4] Q. Hassan et al., "The renewable energy role in the global energy Transformations," Renewable Energy Focus, vol. 48, p. 100545, 2024, doi: https://doi.org/10.1016/j.ref.2024.100545.

[5] T.-Z. Ang, M. Salem, M. Kamarol, H. S. Das, M. A. Nazari, and N. Prabaharan, "A comprehensive study of renewable energy sources: Classifications, challenges and suggestions," Energy Strategy Reviews, vol. 43, p. 100939, 2022, doi: https://doi.org/10.1016/j.esr.2022.100939.

[6] A. G. Olabi et al., "Renewable energy systems: Comparisons, challenges and barriers, sustainability indicators, and the contribution to UN sustainable development goals," International Journal of Thermofluids, vol. 20, p. 100498, 2023, doi: https://doi.org/10.1016/j.ijft.2023.100498.

[7] X. S. Musonye, B. Davíðsdóttir, R. Kristjánsson, E. I. Ásgeirsson, and H. Stefánsson, "Integrated energy systems' modeling studies for sub-Saharan Africa: A scoping review," Renewable and Sustainable Energy Reviews, vol. 128, p. 109915, 2020, doi: https://doi.org/10.1016/j.rser.2020.109915.

[8] G. Nagababu, H. Jani, and H. Puppala, "Harnessing Solar Energy for Sustainable Development of Livelihoods," in Handbook of Climate Change Mitigation and Adaptation, M. Lackner, B. Sajjadi, and W.-Y. Chen, Eds., New York, NY: Springer New York, 2025, pp. 1–36. doi: 10.1007/978-1-4614-6431-0_113-2.

[9] S. Zeng, Y. Liu, C. Liu, and X. Nan, "A review of renewable energy investment in the BRICS countries: History, models, problems and solutions," Renewable and Sustainable Energy Reviews, vol. 74, pp. 860–872, 2017, doi: https://doi.org/10.1016/j.rser.2017.03.016.

[10] Q. Lin, A. Armin, R. C. R. Nagiri, P. L. Burn, and P. Meredith, "Electro-optics of perovskite solar cells," Nat Photonics, vol. 9, no. 2, pp. 106–112, 2015, doi: 10.1038/nphoton.2014.284.

[11] S. Khatoon et al., "Perovskite solar cell's efficiency, stability and scalability: A review," Mater Sci Energy Technol, vol. 6, pp. 437–459, 2023, doi: https://doi.org/10.1016/j.mset.2023.04.007.

[12] D. Zhou, T. Zhou, Y. Tian, X. Zhu, and Y. Tu, "Perovskite-Based Solar Cells: Materials, Methods, and Future Perspectives," 2018, Hindawi Limited. doi: 10.1155/2018/8148072.

[13] N. K. Elangovan, R. Kannadasan, B. B. Beenarani, M. H. Alsharif, M.-K. Kim, and Z. Hasan Inamul, "Recent developments in perovskite materials, fabrication techniques, band gap engineering, and the stability of perovskite solar cells," Energy Reports, vol. 11, pp. 1171–1190, 2024, doi: https://doi.org/10.1016/j.egyr.2023.12.068.

[14] D. B. Mitzi, S. Wang, C. A. Feild, C. A. Chess, and A. M. Guloy, "Conducting Layered Organic-inorganic Halides Containing 〈110〉 -Oriented Perovskite Sheets," Science (1979), vol. 267, no. 5203, pp. 1473–1476, Mar. 1995, doi: 10.1126/science.267.5203.1473.

[15] K. Sharma, V. Sharma, and S. S. Sharma, "Dye-Sensitized Solar Cells: Fundamentals and Current Status," 2018, Springer New York LLC. doi: 10.1186/s11671-018-2760-6.

[16] G. Pindolia, S. M. Shinde, and P. K. Jha, "Optimization of an inorganic lead free RbGeI3 based perovskite solar cell by SCAPS-1D simulation," Solar Energy, vol. 236, pp. 802–821, 2022, doi: https://doi.org/10.1016/j.solener.2022.03.053.

[17] A. A. Zaky et al., "Enhancing efficiency and decreasing photocatalytic degradation of perovskite solar cells using a hydrophobic copper-modified titania electron transport layer," Appl Catal B, vol. 284, p. 119714, 2021, doi: https://doi.org/10.1016/j.apcatb.2020.119714.

[18] C. Devi and R. Mehra, "Device simulation of lead-free MASnI3 solar cell with CuSbS2 (copper antimony sulfide)," J Mater Sci, vol. 54, no. 7, pp. 5615–5624, 2019, doi: 10.1007/s10853-018-03265-y.

[19] T. R. Lenka, A. C. Soibam, K. Dey, T. Maung, and F. Lin, "Numerical analysis of high-efficiency lead-free perovskite solar cell with NiO as hole transport material and PCBM as electron transport material," CSI Transactions on ICT, vol. 8, no. 2, pp. 111–116, Jun. 2020, doi: 10.1007/s40012-020-00291-7.

[20] U. Mandadapu, S. V. Vedanayakam, K. Thyagarajan, M. R. Reddy, and B. Jagadeeshbabu, "Design and Simulation of High Efficiency Tin Halide Perovskite Solar Cell," International Journal of Renewable Energy Research, 2017, [Online]. Available: https://api.semanticscholar.org/CorpusID:139662058

[21] A. Sunny, S. Rahman, M. M. Khatun, and S. R. Al Ahmed, "Numerical study of high performance HTL-free CH3NH3SnI3-based perovskite solar cell by SCAPS-1D," AIP Adv, vol. 11, no. 6, Jun. 2021, doi: 10.1063/5.0049646.

[22] K. Afridi, M. Noman, and S. T. Jan, "Evaluating the influence of novel charge transport materials on the photovoltaic properties of MASnI3 solar cells through SCAPS-1D modelling," R Soc Open Sci, vol. 11, no. 1, p. 231202, Jan. 2024, doi: 10.1098/rsos.231202.

[23] K. Deepthi Jayan and V. Sebastian, "Comprehensive device modelling and performance analysis of MASnI3 based perovskite solar cells with diverse ETM, HTM and back metal contacts," Solar Energy, vol. 217, pp. 40–48, Mar. 2021, doi: 10.1016/j.solener.2021.01.058.

[24] S. Imani, S. M. Seyed-Talebi, J. Beheshtian, and E. W. G. Diau, "Simulation and characterization of CH3NH3SnI3-based perovskite solar cells with different Cu-based hole transporting layers," Appl Phys A Mater Sci Process, vol. 129, no. 2, Feb. 2023, doi: 10.1007/s00339-023-06428-0.

[25] R. Jaiswal et al., "Numerical study of eco-friendly Sn-based Perovskite solar cell with 25.48% efficiency using SCAPS-1D," Journal of Materials Science: Materials in Electronics, vol. 34, no. 8, p. 753, 2023, doi: 10.1007/s10854-023-10171-w.

[26] M. K. Hossain et al., "Numerical simulation and optimization of a CsPbI3-based perovskite solar cell to enhance the power conversion efficiency," New Journal of Chemistry, vol. 47, no. 10, pp. 4801–4817, Jan. 2023, doi: 10.1039/d2nj06206b.

[27] A. K. Chaudhary, S. Verma, and R. K. Chauhan, "Thermal and power performance optimization of cost-effective solar cells using eco-friendly perovskite materials," Phys Scr, vol. 99, no. 2, p. 025512, 2024, doi: 10.1088/1402-4896/ad196e.

[28] M. Burgelman, K. Decock, S. Khelifi, and A. Abass, "Advanced electrical simulation of thin film solar cells," Thin Solid Films, vol. 535, pp. 296–301, 2013, doi: https://doi.org/10.1016/j.tsf.2012.10.032.

[29] M. Burgelman, P. Nollet, and S. Degrave, "Modelling polycrystalline semiconductor solar cells," Thin Solid Films, vol. 361–362, pp. 527–532, 2000, doi: https://doi.org/10.1016/S0040-6090(99)00825-1.

[30] M. S. Uddin et al., "Lead-free Ge-based perovskite solar cell incorporating TiO2 and Cu2O charge transport layers harnessing over 25% efficiency," Journal of Optics, 2023, doi: 10.1007/s12596-023-01570-7.

[31] R. A. Jabr, M. Hamad, and Y. M. Mohanna, "Newton-Raphson Solution of Poisson's Equation in a Pn Diode," International Journal of Electrical Engineering & Education, vol. 44, no. 1, pp. 23–33, Jan. 2007, doi: 10.7227/IJEEE.44.1.3.

[32] F. Saeed and H. E. Gelani, "Unravelling the effect of defect density, grain boundary and gradient doping in an efficient lead-free formamidinium perovskite solar cell," Opt Mater (Amst), vol. 124, p. 111952, 2022, doi: https://doi.org/10.1016/j.optmat.2021.111952.

[33] A. Rahmoune and O. Babahani, "Numerical analysis of Al/Gr/ETL/MoS2/Sb2S3/Ni solar cell using non-toxic In2S3/SnS2/ZnSe electron transport layer," Optik (Stuttg), vol. 283, p. 170875, 2023, doi: https://doi.org/10.1016/j.ijleo.2023.170875.

[34] S. Goutham Kumar, E. A. R, T. Surya Teja Reddy, P. C. R, and G. V Honnavar, "Performance Analysis and Optimization of Lead-Free Tin-Based MASnBr3 Tandem Perovskite Solar Cell Section A-Research paper PERFORMANCE ANALYSIS AND OPTIMIZATION OF LEAD-FREE TIN-BASED MASnBr3 TANDEM PEROVSKITE SOLAR CELL," Chem. Bull, vol. 12, no. 6, pp. 2814–2832, 2023, doi: 10.31838/ecb/2023.12.6.251.

[35] Z. Khan, M. Noman, S. Tariq Jan, and A. Daud Khan, "Systematic investigation of the impact of kesterite and zinc based charge transport layers on the device performance and optoelectronic properties of ecofriendly tin (Sn) based perovskite solar cells," Solar Energy, vol. 257, pp. 58–87, 2023, doi: https://doi.org/10.1016/j.solener.2023.04.019.

[36] P. K. Patel, "Device simulation of highly efficient eco-friendly CH3NH3SnI3 perovskite solar cell," Sci Rep, vol. 11, no. 1, p. 3082, 2021, doi: 10.1038/s41598-021-82817-w.

[37] P. Lopez-Varo et al., "Dynamic temperature effects in perovskite solar cells and energy yield," Sustain Energy Fuels, vol. 5, no. 21, pp. 5523–5534, 2021, doi: 10.1039/D1SE01381E.

[38] D. Shi et al., "Low trap-state density and long carrier diffusion in organolead trihalide perovskite single crystals," Science (1979), vol. 347, no. 6221, pp. 519–522, Jan. 2015, doi: 10.1126/science.aaa2725.

[39] G. Hodes and P. V Kamat, "Understanding the Implication of Carrier Diffusion Length in Photovoltaic Cells," J Phys Chem Lett, vol. 6, no. 20, pp. 4090–4092, Oct. 2015, doi: 10.1021/acs.jpclett.5b02052.

[40] J. Burschka et al., "Sequential deposition as a route to high-performance perovskite-sensitized solar cells," Nature, vol. 499, no. 7458, pp. 316–319, 2013, doi: 10.1038/nature12340.

[41] B. Yang et al., "CuSbS2 as a Promising Earth-Abundant Photovoltaic Absorber Material: A Combined Theoretical and Experimental Study," Chemistry of Materials, vol. 26, no. 10, pp. 3135–3143, May 2014, doi: 10.1021/cm500516v.

[42] H. Y. Yang, W. Y. Rho, S. K. Lee, S. H. Kim, and Y. B. Hahn, "TiO 2 nanoparticles/nanotubes for efficient light harvesting in perovskite solar cells," Nanomaterials, vol. 9, no. 3, Mar. 2019, doi: 10.3390/nano9030326.

[43] F. Liu et al., "Numerical simulation: Toward the design of high-efficiency planar perovskite solar cells," Appl Phys Lett, vol. 104, no. 25, p. 253508, Jun. 2014, doi: 10.1063/1.4885367.

[44] A. Bag, R. Radhakrishnan, R. Nekovei, and J. Ramanujam, "Effect of absorber layer, hole transport layer thicknesses, and its doping density on the performance of perovskite solar cells

by device simulation," Solar Energy, vol. 196, pp. 177–182, Aug. 2020, doi: 10.1016/j.solener.2019.12.014.

[45] N. J. Valeti, K. Prakash, and M. K. Singha, "Numerical simulation and optimization of lead free CH3NH3SnI3 perovskite solar cell with CuSbS2 as HTL using SCAPS 1D," Results in Optics, vol. 12, Jul. 2023, doi: 10.1016/j.rio.2023.100440.

[46] M. K. Hossain et al., "Harnessing the potential of CsPbBr3-based perovskite solar cells using efficient charge transport materials and global optimization," RSC Adv, vol. 13, no. 30, pp. 21044–21062, Jul. 2023, doi: 10.1039/d3ra02485g.

[47] Y. Raoui, H. Ez-Zahraouy, N. Tahiri, O. El Bounagui, S. Ahmad, and S. Kazim, "Performance analysis of MAPbI3 based perovskite solar cells employing diverse charge selective contacts: Simulation study," Solar Energy, vol. 193, pp. 948–955, Nov. 2019, doi: 10.1016/j.solener.2019.10.009.

[48] M. Li et al., "CdTe Nanocrystal Hetero-Junction Solar Cells with High Open Circuit Voltage Based on Sb-doped TiO2 Electron Acceptor Materials," Nanomaterials, vol. 7, no. 5, 2017, doi: 10.3390/nano7050101.

[49] O. Ahmad, A. Rashid, M. W. Ahmed, M. F. Nasir, and I. Qasim, "Performance evaluation of Au/p-CdTe/Cs2TiI6/n-TiO2/ITO solar cell using SCAPS-1D," Opt Mater (Amst), vol. 117, p. 111105, 2021, doi: https://doi.org/10.1016/j.optmat.2021.111105.

[50] Y. H. Khattak, F. Baig, S. Ullah, B. Marí, S. Beg, and H. Ullah, "Enhancement of the conversion efficiency of thin film kesterite solar cell," Journal of Renewable and Sustainable Energy, vol. 10, no. 3, p. 033501, May 2018, doi: 10.1063/1.5023478.

[51] T. Leijtens et al., "Carrier trapping and recombination: the role of defect physics in enhancing the open circuit voltage of metal halide perovskite solar cells," Energy Environ. Sci., vol. 9, no. 11, pp. 3472–3481, 2016, doi: 10.1039/C6EE01729K.

[52] I. Alam, R. Mollick, and M. A. Ashraf, "Numerical simulation of Cs2AgBiBr6-based perovskite solar cell with ZnO nanorod and P3HT as the charge transport layers," Physica B Condens Matter, vol. 618, p. 413187, 2021, doi: https://doi.org/10.1016/j.physb.2021.413187.

[53] L. Lin, L. Jiang, P. Li, B. Fan, and Y. Qiu, "A modeled perovskite solar cell structure with a Cu2O hole-transporting layer enabling over 20% efficiency by low-cost low-temperature processing," Journal of Physics and Chemistry of Solids, vol. 124, pp. 205–211, 2019, doi: https://doi.org/10.1016/j.jpcs.2018.09.024.

[54] R. Jeyakumar, A. Bag, R. Nekovei, and R. Radhakrishnan, "Influence of Electron Transport Layer (TiO2) Thickness and Its Doping Density on the Performance of CH3NH3PbI3-Based Planar Perovskite Solar Cells," J Electron Mater, vol. 49, no. 6, pp. 3533–3539, Jun. 2020, doi: 10.1007/s11664-020-08041-w.

[55] U. Mandadapu, S. V. Vedanayakam, and K. Thyagarajan, "Simulation and Analysis of Lead based Perovskite Solar Cell using SCAPS-1D," Indian J Sci Technol, vol. 10, no. 11, pp. 1–8, Mar. 2017, doi: 10.17485/ijst/2017/v10i11/110721.

[56] Y. Cao et al., "Towards high efficiency inverted Sb2Se3 thin film solar cells," Solar Energy Materials and Solar Cells, vol. 200, Sep. 2019, doi: 10.1016/j.solmat.2019.109945.

[57] R. Chakraborty, K. M. Sim, M. Shrivastava, K. V Adarsh, D. S. Chung, and A. Nag, "Colloidal Synthesis, Optical Properties, and Hole Transport Layer Applications of Cu2BaSnS4 (CBTS) Nanocrystals," ACS Appl Energy Mater, vol. 2, no. 5, pp. 3049–3055, May 2019, doi: 10.1021/acsaem.9b00473.

[58] Y. H. Khattak, F. Baig, H. Toura, S. Beg, and B. M. Soucase, "CZTSe Kesterite as an Alternative Hole Transport Layer for MASnI3 Perovskite Solar Cells," J Electron Mater, vol. 48, no. 9, pp. 5723–5733, 2019, doi: 10.1007/s11664-019-07374-5.

[59] U. Mandadapu, "Simulation and Analysis of Lead based Perovskite Solar Cell using SCAPS-1D," Indian J Sci Technol, vol. 10, no. 1, pp. 1–8, Jan. 2017, doi: 10.17485/ijst/2017/v11i10/110721.

[60] F. Anwar, R. Mahbub, S. S. Satter, and S. M. Ullah, "Effect of Different HTM Layers and Electrical Parameters on ZnO Nanorod-Based Lead-Free Perovskite Solar Cell for High-Efficiency Performance," International Journal of Photoenergy, vol. 2017, 2017, doi: 10.1155/2017/9846310.

[61] G. E. Eperon et al., "Inorganic caesium lead iodide perovskite solar cells," J Mater Chem A Mater, vol. 3, no. 39, pp. 19688–19695, 2015, doi: 10.1039/C5TA06398A.

[62] J. Hossain, Md. M. A. Moon, B. K. Mondal, and M. A. Halim, "Design guidelines for a highly efficient high-purity germanium (HPGe)-based double-heterojunction solar cell," Opt Laser Technol, vol. 143, p. 107306, 2021, doi: https://doi.org/10.1016/j.optlastec.2021.107306.

[63] S. R. I. Biplab, Md. H. Ali, Md. M. A. Moon, Md. F. Pervez, Md. F. Rahman, and J. Hossain, "Performance enhancement of CIGS-based solar cells by incorporating an ultrathin BaSi2 BSF layer," J Comput Electron, vol. 19, no. 1, pp. 342–352, 2020, doi: 10.1007/s10825-019-01433-0.

[64] C. M. Proctor and T. Q. Nguyen, "Effect of leakage current and shunt resistance on the light intensity dependence of organic solar cells," Appl Phys Lett, vol. 106, no. 8, Feb. 2015, doi: 10.1063/1.4913589.

[65] P. Roy, N. Kumar Sinha, and A. Khare, "An investigation on the impact of temperature variation over the performance of tin-based perovskite solar cell: A numerical simulation approach," Mater Today Proc, vol. 39, pp. 2022–2026, 2021, doi: https://doi.org/10.1016/j.matpr.2020.09.281.

[66] A. Ashfaq et al., "Comparative performance analysis of Cs2TiX6 (X = Br-, Cl-, I-) lead-free perovskite solar cells incorporating single, double and triple layer halides by SCAPS −1D," Mater Today Commun, vol. 35, p. 106016, 2023, doi: https://doi.org/10.1016/j.mtcomm.2023.106016.

[67] A. Belasri and S. A. Beldjilali, "Springer Proceedings in Energy," 2020. doi: 10.1007/978-981-15-5444-5.

[68] H. B. Michaelson, "The work function of the elements and its periodicity," J Appl Phys, vol. 48, no. 11, pp. 4729–4733, 1977, doi: 10.1063/1.323539.

[69] Y. H. Khattak, F. Baig, H. Toura, S. Beg, and B. M. Soucase, "CZTSe Kesterite as an Alternative Hole Transport Layer for MASnI3 Perovskite Solar Cells," J Electron Mater, vol. 48, no. 9, pp. 5723–5733, 2019, doi: 10.1007/s11664-019-07374-5.

[70] Y. Gan et al., "Numerical Investigation Energy Conversion Performance of Tin-Based Perovskite Solar Cells Using Cell Capacitance Simulator," Energies (Basel), vol. 13, no. 22, 2020, doi: 10.3390/en13225907.

[71] E. Danladi, A. O. Salawu, M. O. Abdulmalik, E. D. Onoja, E. E. Onwoke, and D. S. Adepehin, "Optimization of Absorber and ETM Layer Thickness for Enhanced Tin based Perovskite Solar Cell Performance using SCAPS-1D Software," Physics Access, vol. 02, no. 01, pp. 1–11, 2022, doi: 10.47514/phyaccess.2022.2.1.001.

[72] M. Tripathi, V. Vaibhav Mishra, B. S. Sengar, and A. V Ullas, "Lead-free perovskite solar cell byUsing SCAPS-1D: Design and simulation," Mater Today Proc, vol. 62, pp. 4327–4331, 2022, doi: https://doi.org/10.1016/j.matpr.2022.04.832.